Rothamsted Repository Download

A - Papers appearing in refereed journals

Blanchy, G., Virlet, N., Sadeghi-Tehran, P., Watts, C. W., Hawkesford, M. J., Whalley, W. R. and Binley, A. 2020. Time-intensive geoelectrical monitoring under winter wheat . *Near Surface Geophysics.*

The publisher's version can be accessed at:

- https://dx.doi.org/10.1002/nsg.12107

The output can be accessed at: https://repository.rothamsted.ac.uk/item/97yv5/time-intensive-geoelectrical-monitoring-under-winter-wheat.

© 18 May 2020, Please contact library@rothamsted.ac.uk for copyright queries.

Time-intensive geoelectrical monitoring under winter wheat

Guillaume Blanchy[1,2]*, Nicolas Virlet[2], Pouria Sadeghi-Tehran[2], Christopher W. Watts[2], Malcolm J. Hawkesford[2], William R. Whalley[2] and Andrew Binley[1]

[1]*Lancaster University, Lancaster, Lancashire LA1 4YW, UK, and* [2]*Rothamsted Research, Harpenden, Hertfordshire AL5 2JQ, UK*

ABSTRACT

Several studies have explored the potential of electrical resistivity tomography to monitor changes in soil moisture associated with the root water uptake of different crops. Such studies usually use a set of limited below-ground measurements throughout the growth season but are often unable to get a complete picture of the dynamics of the processes. With the development of high-throughput phenotyping platforms, we now have the capability to collect more frequent above-ground measurements, such as canopy cover, enabling the comparison with below-ground data. In this study hourly direct-current resistivity data were collected under the Field Scanalyzer platform at Rothamsted Research with different winter wheat varieties and nitrogen treatments in 2018 and 2019. Results from both years demonstrate the importance of applying the temperature correction to interpret hourly electrical conductivity data. Crops which received larger amounts of nitrogen showed larger canopy cover and more rapid changes in electrical conductivity, especially during large rainfall events. The varieties showed contrasted heights although this does not appear to have influenced electrical conductivity dynamics. The daily cyclic component of the electrical conductivity signal was extracted by decomposing the time series. A shift in this daily component was observed during the growth season. For crops with appreciable difference in canopy cover, high-frequency direct-current resistivity monitoring was able to distinguish the different below-ground behaviours. The results also highlight how coarse temporal sampling may affect interpretation of resistivity data from crop monitoring studies.

Key words: Electrical resistivity tomography, Hydrogeophysics, Near-surface.

Highlights

– Hourly electrical resistivity tomography data were collected under a high-throughput field phenotyping platform.
– The dynamics of the electrical conductivity (EC) varied mainly with N treatments and canopy cover.
– We identified a shift in the EC diurnal cycle probably due to the root water uptake.
– Little EC difference between the wheat varieties was observed.

*E-mail: g.blanchy@lancaster.ac.uk

INTRODUCTION

Field phenotyping

Senapati and Semenov (2020) show that European wheat varieties still have genetic potential to be exploited through breeding programs. Traits such as optimal root water uptake are present in the genetic population but still need to be selected and transferred into commercial varieties via crop breeding. To create new varieties with desirable traits (e.g. high yield, short stem and deep rooting), crop breeders cross other varieties which exhibit one or several of the desired traits. This process generates large number of different genotypes (or lines). To select which genotype possesses which

traits, all lines are grown and their respective phenotype (i.e. the combination of all traits) is assessed. The lines which show desired traits are selected and can potentially become new varieties. Although this is a simplistic description of crop breeding techniques, it provides a context for this study.

One of the usual steps to assess crop phenotype is to grow the different lines in large field fields. This step can be labour-intensive due the large number of lines to screen, leading to a `phenotyping bottleneck' (Furbank and Tester, 2011). To relieve it, new tools are being developed (Araus and Cairns, 2014; Atkinson *et al.*, 2019). Among them, automated high-throughput phenotyping platforms permit the collection of many above-ground traits automatically (Prasanna *et al.*, 2013). An example of such infrastructure is the Field Scanalyzer facility at Rothamsted Research (Virlet *et al.*, 2017). Despite this progress, there has been less advance in the development of below-ground methods (Atkinson *et al.*, 2019). Geophysical methods, such as electrical resistivity tomography, electromagnetic induction and ground penetrating radar, have been identified as promising candidates to fill this gap (Araus and Cairns, 2014; Atkinson *et al.*, 2019).

Geoelectrical monitoring in agriculture

Geophysical methods can image near-surface processes at multiple-scales (Binley *et al.*, 2015) and hence have a great potential for agricultural applications, for example, for assessing the spatial and temporal distribution of soil water. Geoelectrical methods, and more specifically electrical resistivity tomography (ERT), has proven useful in imaging variation in soil moisture in several field applications (Michot *et al.*, 2003; Srayeddin and Doussan, 2009; Whalley *et al.*, 2017). ERT data are usually collected at regular time intervals enabling to separate the static and dynamic components of the soil electrical conductivity. The dynamic component is usually dominated by the change in soil moisture caused by various processes, in particular plant water uptake and evaporation. The static component is usually linked to soil textural properties such as clay content. Such time-lapse studies have been used to investigate the root zone moisture interaction for different ecosystems (Jayawickreme *et al.*, 2008). At smaller scales, ERT monitoring has been applied in orchards to investigate, in two dimension (2D) and three dimension (3D), the soil moisture dynamics influenced by the root water uptake and irrigation strategies (Cassiani *et al.*, 2015; Consoli *et al.*, 2017; Vanella *et al.*, 2018). In herbaceous plants, time-lapse ERT was used to determine the spatial pattern of root water uptake of corn and sorghum in irrigated conditions (Srayeddin

and Doussan, 2009) as well as corn with cover crops (Michot et al., 2003). More recently, Coussement *et al.* (2018) used 2D ERT monitoring to measure the effects of a tree border on the soil moisture of a corn field. At the plot scale, Whalley *et al.* (2017) used time-lapse ERT to differentiate root water uptake of different wheat varieties.

All the studies above used time-lapse monitoring which usually involves collecting a few sets of ERT measurements during the growth season of the crop or around specific irrigation events. As such, they provide a few snapshots of the soil electrical conductivity, showing the effects of the seasonal processes. Hourly monitoring over long periods is rare but it has the potential to offer more insight into the dynamics of plant–soil–water interactions. For example, Vanella *et al.* (2018) use hourly 3D ERT monitoring to image the effects of full irrigation and partial root zone drying on an orange tree. They highlight that access to time-intensive monitoring provides more information on the soil moisture dynamics than less frequent measurements under specific transient conditions. Mares *et al.* (2016) linked the diurnal pattern of soil electrical conductivity with the sap flow movement in pine trees. At the laboratory scale, Werban *et al.* (2008) monitored at hourly intervals the soil moisture beneath a lupin plant using 2D ERT and estimated the root water uptake of the plant. In addition to being able to follow the dynamics of specific events, hourly measurements have the potential to look at daily dynamics. Finally, another advantage of hourly scale sampling is that it is closer to the scale at which physiological processes of the plant take place. Given the wide availability of automated monitoring ERT instrumentation, high-frequency below-ground geophysical measurements may offer more information for crop breeding studies.

To analyse the value of geoelectrical monitoring under high-throughput phenotying

platform in a phenotyping context, this paper focuses on the following research questions. (i) What is the potential of geophysical tools for monitoring below-ground dynamics? (ii) How can geophysically derived below-ground information be linked to above-ground traits dynamics? (iii) What are the capabilities and limitations of geoelectrical monitoring for phenotyping applications?

MATERIALS AND METHODS

Experimental setup

The experiments were carried out at Rothamsted Research, United Kingdom (51°48′34.56″N, 0°21′22.68″W) in Great

Field, under the Field Scanalyzer platform area (Virlet *et al.*, 2017). The platform covers a flat area of 0.12 ha. The soil is described as a Luvisol (WRB) and is composed of a loamy top layer (0.3 m) over a more clayey layer with flints (Batcombe). The soil drainage can be impeded by this second layer especially in the areas around the platform due to heavy traffic during the construction. Two experiments were conducted during the growing season in 2017–2018 (hereafter referred to as 2018) and 2018–2019 (hereafter referred to as 2019) under rainfed conditions.

In 2018, three different varieties of winter wheat (*Triticum aestivum* L. var. Mercia Rht3, Mercia RhtC and Shamrock) were sown on 2017-10-30 (all dates are expressed in ISO 8601 format) in `sowing plots' of 0.6 m length by 1 m width with a planting density of 350 seeds/m$^2$ and were grown under normal UK nitrogen rate (~200 kgN/ha). Each `sowing plot', made up of two subplots, 0.6 m by 0.5 m, was sown with the same variety. Two continuous `sowing plots' of the same variety were grouped to form a plot unit for this experimentation. This design was inherited from a larger experiment taking place in the same field. Each plot was equipped with 10 stainless steel electrodes of 0.1 m length with 0.15 m inter-electrode spacing. The electrodes were entirely buried (end of the electrode at 0.1 m below the surface) between the rows of wheat, hence not in contact with the plants. The pins of two nearby plots were attached to an array of 24 pins (four pins were discarded). The two electrical resistivity tomography (ERT) arrays were connected to an ERT monitoring system. The aim of this experiment was to identify any differences in soil electrical conductivity between the varieties.

In 2019, four plots of a nitrogen/variety trial sown on 2018-10-25 were equipped with an ERT array. Two varieties, Crusoe and Istabraq, were grown in plot of 3 m by 1 m under low and high nitrogen fertilization (50 kgN/ha and 350 kgN/ha as dry pellets, respectively). The first application of nitrogen 50 kgN/ha was made on 2019-03-08 and the second application was made on 2019-04-10. Figure 1 shows the four plots being monitored. Each plot was equipped of 12 stainless steel electrodes of 0.1 m length with 0.3 m inter-electrode spacing. As in the 2018 setup, the electrodes were entirely buried between the rows of wheat, avoiding contact with the plants. The pins of two nearby plots were attached to a 24 pins array that was connected to the ERT monitoring system.

Above-ground variables

The above ground data were collected by the Field Scanalyzer platform (Virlet *et al.*, 2017). The growth parameters were collected from RGB (Red Green Blue) camera (Prosilica GT3300, Allied Vision, 3296 × 2472 pixels) for the canopy cover and from the 3D laser scanner (Fraunhofer Institute, Munich, Germany) for height.

Canopy cover values were derived from the RGB images and expressed as a percentage of the image covered by green pixels belonging to the plot canopy (Sadeghi-Tehran *et al.*, 2017). The height of the crop was obtained from the three-dimensional cloud points using the 98th percentile of the vertical coordinates of the cloud points (adapting from Lyra *et al.*, unpublished). The height and canopy cover of the crops were available for both 2018 and 2019.

Geophysical data processing

Electrical resistivity tomography

Electrical resistivity tomography (ERT) measurements were collected using a remotely controlled Syscal Pro 48 (Iris Instruments, Orléans, France) at hourly intervals. In both years, the measurement sequence used was a dipole–dipole configuration (using one and two electrode spacing between the current/potential dipole and, respectively, eight and six levels between the current and potential dipoles) with electrode spacing of 0.15 m (2018) and 0.3 m (2018). Reciprocal measurements were included in the sequence after each normal set. Additional dummy quadrupoles (40 for the entire sequence) were also added to optimize the sequence (specific to the Syscal instrument); in total, the sequence for both years was composed of 496 quadrupoles (124 per plot).

In 2018, the system was operational between the end of May and July to capture rainfall events when the wheat was fully mature (between flowering and harvest). In 2019, the ERT monitoring system ran successfully from February to the end of August (flowering around 14th June) with a few data gaps. At the end of May, current injection errors were noted and so the instrument was replaced with another Syscal Pro 48 to allow monitoring until September. We noticed that the data from this second device had higher reciprocal errors than the original one, in particular, for larger dipoles. Despite this, the datasets from both instruments show consistency in dynamics by reacting to rainfall events and showing similar daily fluctuations.

The ERT data collected were processed using the ResIPy software (Blanchy *et al.*, 2020) that makes use of the Occam's based R2 inversion code (Binley, 2015). Because of the short electrode spacing compared to the length of the electrode, the nodes of the mesh corresponding to the electrode were
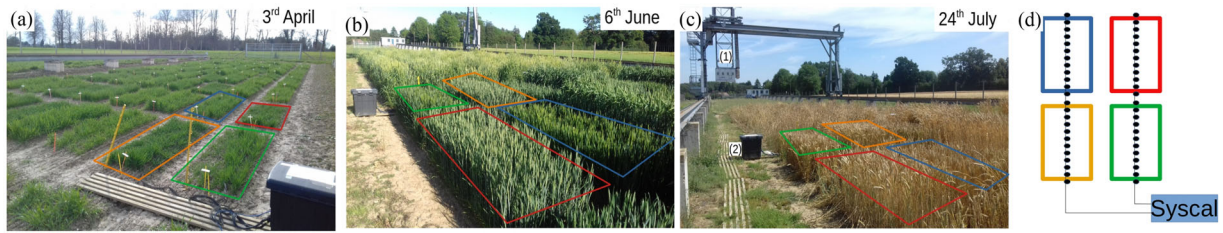
Figure 1 Photographs of the experiment under the Field Scanalyzer facility at Rothamsted Research in (a) April, (b) June and (c) July 2019. (c) The box containing the different sensors (marked (1) and black box marked (2) contains the ERT monitoring system connected to arrays in the four plots. The variety and nitrogen treatment of the plots are identified by coloured rectangles: (blue) Crusoe 50 kgN/ha, (orange) Istabraq 350 kgN/ha, (green) Crusoe 350 kgN/ha and (red) Istabraq 50 kgN/ha.) (d) The plan of the installation for 2019.

positioned at 60% of the electrode length (Rücker and Günther, 2011). Given the relatively small number of quadrupoles per plot, surveys were combined in batches of 24 (a day) and a power-law error model was fitted for each batch using the binned reciprocal errors. This approach ensures a sufficient number of data points to obtain a robust error model, while allowing the error model to vary throughout the season. Each dataset was then inverted independently in a batch mode. The difference inversion method of LaBrecque and Yang (2001) did not work well for our dataset when applied over the entire season either using a single background survey or applied over consecutive surveys. For 2019, it produced satisfactory results until May, before large changes in electrical conductivity occurred. After May 2019, the difference approach was not able to reproduce the small variations in electrical conductivity observed at hourly intervals in the apparent data. This was partly due to the higher reciprocal errors observed after May that forces the inversion towards a smooth solution. Inverting independent surveys and constraining them to the background survey produced better results for the earlier dates. However, after May 2019, this approach produced inverted sections that were too biased towards the background image. For this reason, we decided to invert each survey independently with its own error model. Although this approach does not take advantage of difference or background regularization option that could potentially reduce time-lapse artefacts, it still produces inversions that show clear temporal dynamics. Each inverted section was then averaged into a one-dimensional (1D) profiles per plot used in the rest of the study. The 1D profiles were computed for ease of comparison between plots.

Electrical conductivity temperature correction

It is essential that the temperature correction is applied to be able to distinguish between soil moisture and temperature effects on electrical conductivity. The variation in bulk electrical conductivity with temperature is due primarily to two factors: the change in the ion mobility and the change in the viscosity of the pore water (Hayley *et al.*, 2007). To account for the effect of temperature, different models have been developed. Ma *et al.* (2011) compared the different corrections found in the literature and concluded that a ratio model performs well in the range 3–47°C. Beyond this range, the empirical model proposed by Sheets and Hendrickx (1995), which appears in the corrected form in Corwin and Lesch (2005), is more appropriate. Hayashi (2004) explored the range of applicability of the ratio model and concluded that this model is applicable within the 0–30°C temperature range, which is similar to the conclusion of Ma *et al.* (2011).

Given that our soil temperature lies within the 0–30°C range, we applied the ratio model to our data with a 2% increase per degree:

$$\sigma_{25} = \frac{\sigma_T}{1 + 0.02 \times (T - 25)}, \tag{1}$$

where σ_{25} is the equivalent electrical conductivity at 25°C, σ_T is the bulk electrical conductivity measured at the temperature T in° C. Note that this model makes the correction factor dependent on σ_{25}. For our study, we used the hourly soil temperature values measured at five depths (0.1, 0.2, 0.3, 0.5 and 1 m) under grass from the Rothamsted weather station (e-RA Rothamsted electronic archive) located about 100 m from the experimental plots. The temperatures were linearly interpolated with depth to match the depths of the inverted electrical conductivities. All inverted conductivity values presented hereafter have been temperature corrected using this relationship.

Time series analysis

The decomposition of the time series of electrical conductivities was applied to the 2019 dataset because it is longer

and allows analysis of seasonal change (not possible with the shorter 2018 dataset). For a selected depth, the series of interest is composed of temperature corrected inverted electrical conductivities from February to September 2019. The signal is broken down into three components using an additive model:

$$Y(t) = T(t) + S(t) + e(t), \qquad (2)$$

where $Y(t)$ represent the raw signal, $T(t)$ represent the trend, $S(t)$ is the daily component, $e(t)$ is the residual. All components are dependent on time t. Note that the daily component is sometimes referred as the seasonality of the time series and represents repeating short-term cycles in the series. This decomposition is simple but enables the identification of different aspects of the signal. To decompose the signal, the algorithm proceeds as follows:

1 The period of the short-term cycles of the signal is identified. In this case, the signal shows a short-term cycle every 24 hours (daily).
2 A moving average is applied on the series with a window size corresponding to this period, this produces the trend.
3 The trend is subtracted from the raw signal and the resulting values are averaged for each period to form the daily component.
4 The residuals are obtained by subtracting the trend and the daily components from the raw data.

The algorithm was implemented using the 'seasonal_decompose()' function of the *statsmodels* Python package (Seabold and Perktold, 2010).

RESULTS

Effect of the soil temperature variations

Figure 2 shows the impact of the temperature correction by analysing the cross-correlation between the soil temperature at 0.15 m depth and the corresponding averaged inverted conductivity from the plot of Crusoe 50 kgN/ha. The temperature correction has two main effects. First, it increases the overall electrical conductivity to bring it to an equivalent electrical conductivity at 25°C. That allows us to compare different dates throughout the season. Second, it decreases the cross-correlation between the two variables.

Inverted profiles

Figure 3 shows examples of the inverted resistivity section and their corresponding averaged inverted conductivity profiles for 2018 and 2019 experiments. For a given year, all profiles show similar values and pattern due to the proximity of the plots.

Seasonal variations

Figures 4 and 5 illustrate the time course of the different variables during the 2018 and 2019 experiments. In 2018, the electrical resistivity tomography (ERT) monitoring system successfully captured a large rainfall event that took place at the end of May. All varieties reached full canopy cover at the end of May and maximal height around mid-June. Figure 4(d) shows clearly the large increase in electrical conductivity due to the rainfall and the progressive soil drying afterwards. This effect is strongly attenuated at the depth of 0.44 m (Fig. 4e). The daily averaged rates of decrease in electrical conductivity at 0.22 m between 2018-06-05 and 2018-07−01 are −0.12 m.S^{-1}.d^{-1}(Mercia Rht3), −0.10 m.S^{-1}.d^{-1}(Shamrock) and −0.15 m.S^{-1}.d^{-1} (Mercia RhtC). Figure 4(c) shows clearly the different heights of the varieties with Mercia Rht3 being a dwarf variety while Mercia RhtC is a tall variety.

Figure 5 shows the time course of the different variables collected in 2019. Figure 5(a) shows daily precipitation and potential soil moisture deficit (PSMD). The PSMD was obtained from meteorological variables measured at the Harpenden weather station (full methodology at: http://www.era.rothamsted.ac.uk/Met/derived_variables#PSMD). From the end of April, the canopy cover of the two high N plots exceeded the canopy cover of the low N plots and reached a maximum by mid-June, irrespectively of the variety (Fig. 5b). The canopy cover started to decrease in the beginning of July as an effect of the senescence. In contrast, the height of the crops appears to be related to the variety and less influenced by the nitrogen treatments (Fig. 5c). Note, however, that Istabraq 50 kgN/ha is slightly smaller than Istabraq 350 kgN/ha at the end of the season.

Figure 5(d,e) shows the temperature corrected inverted conductivity at depths of 0.15 m and 0.45 m, respectively. The shallower depth (Fig. 5d) shows a peak around 2019-03-20 after the first application of fertilizer and then the electrical conductivity of all four plots starts to decrease coinciding with the measured increase in canopy cover. Two other peaks can be observed around 2019-05-10 and 2019-06-25 after significant rainfall events (Fig. 5a). During these two events, Istabraq 350 kgN/ha and Crusoe 350 kgN/ha show larger increases in conductivity but also a more rapid decrease over the following days. A later rainfall event occurred at the end of August but
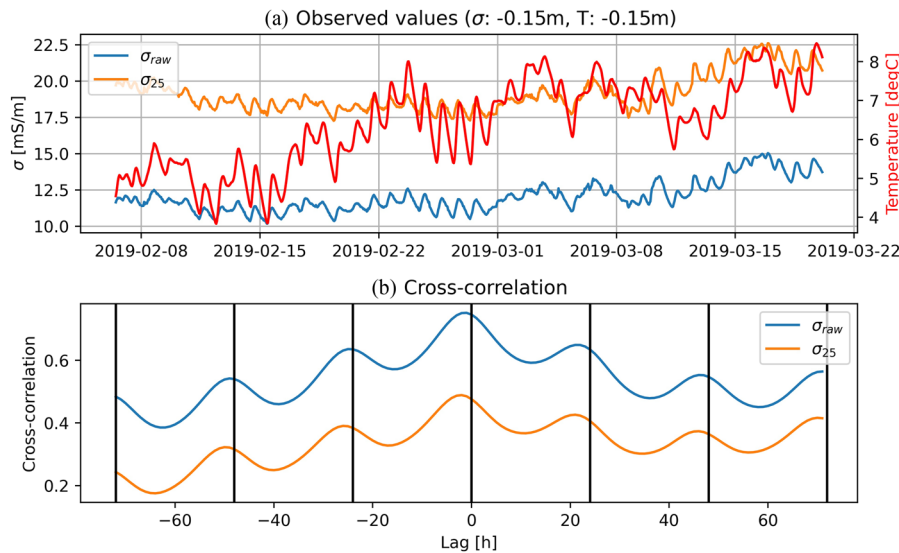
Figure 2 (a) Example inverted conductivities values with and without the temperature correction. (b) Cross-correlation between the inverted electrical conductivity (corrected or not) and the soil temperature at 0.15 m depth. The inverted conductivities are extracted from the Crusoe 50 kgN/ha plot of the 2019 experiment. Similar graphs can be observed on the other plots.

no dramatic decrease in conductivity is seen following this as the crop has been harvested mid-August. The slight decrease observed could be attributed to the usual drying of the soil. The deeper depth presented in Figure 5(e) shows a more attenuated response to that in Figure 5(d): no clear difference between the nitrogen treatments or the varieties can be seen. However, the two major rainfall events of 2019-05-10 and 2019-06-25 appear to drive a slight increase in electrical conductivity at depth, albeit much weaker than that seen at the shallow depth. Note also the increase in electrical conductivity for Crusoe 350 kgN/ha around 2019-03-20 at −0.45 m.

Time series analysis

Figure 6 shows the decomposition of a selected portion of the temperature-corrected and inverted conductivity curves during the first rainfall event, May 2019. The observed signal (Fig. 6a) comprised a general trend (Fig. 6b), a daily component (Fig. 6c) and a residual component (Fig. 6d) using the additive model described earlier. The diurnal characteristic of the signal is clearly shown by this analysis (Fig. 6c) decreasing during the day and increasing during the night (shaded areas). This cycle is common to all four plots in May 2019.

The same additive decomposition can be applied to different moving time windows of seven days with two-day offsets between the windows. The daily component extracted is shown for each window in Figure 7 for the 0.15 m depth. The advantage of applying the decomposition on smaller time

windows compared to the whole signal is that it allows us to see the evolution of the daily component through the season. In Figure 7, it can be seen that the lower part of the daily component (strong blue), initially around 6h00 in February progressively shifts down to 17h00 by the end of April, when the crops start to grow a mature canopy and extract more water from the soil. This shift is subtle but consistent among consecutive weeks. Note as well that in February and March (Fig. 7b,c), the decrease in electrical conductivity occurs mainly during the night which is the opposite of what is observed later in the season, in May, for instance (Fig. 6c).

Reaction to rainfall event

Figure 8 shows an enlarged graph during a major rainfall event at the end of May 2019. It illustrates how the shallow electrical conductivity of the two crops which, received larger amounts of nitrogen fertilizer, increase immediately after the large rainfall and then decrease at a greater rate over the following days. The average decrease rates in electrical conductivity are computed between 2019-05-11 and 2019-05-29 for each plot. When grouped by N treatments, high N plots decrease faster (-0.47 mS.m^{-1}.d^{-1}) than low N plots (-0.15 mS.m^{-1}.d^{-1}). This behaviour was mainly observed at depths shallower than 0.2 m. The rates of decrease in electrical conductivity of the four plots correlated well ($R^2 = 0.57$) with their respective maximum canopy covers (Fig. 5b) but not with their heights ($R^2 < 0.01$). Subsequent (albeit smaller)
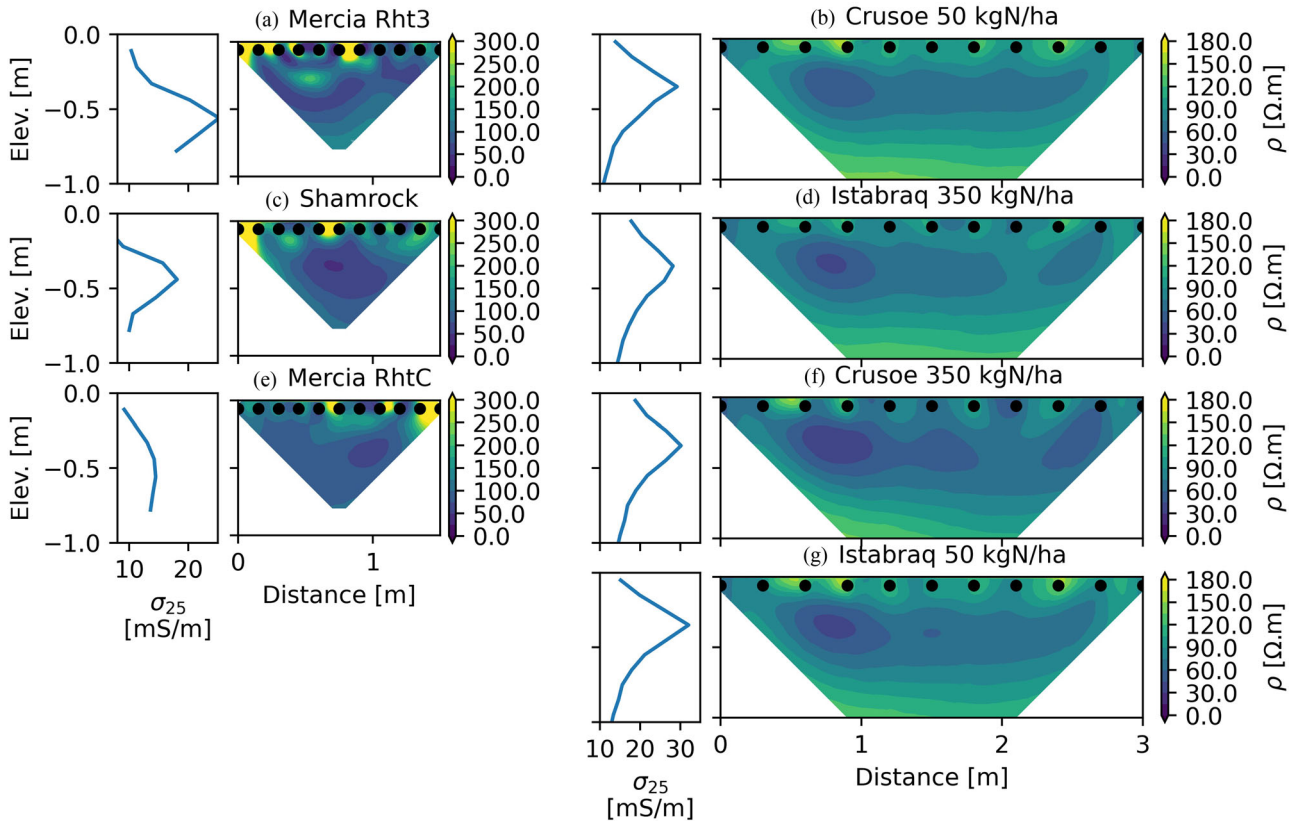
Figure 3 Inverted resistivity sections and their corresponding temperature corrected averaged 1D profile for the three plots in 2018 (a, c and e) and the four plots in 2019 (b, d, f and g) (both taken on 15th June). Note that the resistivity and conductivity scales are different between 2018 and 2019.

rainfalls do not have any visible impact on the electrical conductivity.

Yield

For each year, the grain and straw dry weights were measured and converted to yield in t/ha at 85% dry matter (Table 1). The yield in 2018 was much smaller compared to 2019. This can be explained by the lack of rain in 2018 and several bird damages. In 2018, Mercia RhtC (tall variety) had the largest grain and straw yield while Mercia Rht3 (dwarf variety) had the lowest. In 2019, the two plots which received more nitrogen fertilizer had a higher grain and straw yield compared to those which only received one application of fertilizer. For the same rate of nitrogen fertilizer, Istabraq had higher yield than Cruose. In 2018, there was no clear relationship between the grain yield and the daily rate of decrease in shallow electrical conductivity after the large rainfall event ($R^2 = 0.08$). In contrast, in 2019, larger grain yield was associated with larger daily rate of decrease in shallow electrical

conductivity after the major rainfall event at the end of May ($R^2 = 0.52$).

DISCUSSION

Implementation of geoelectrical monitoring

The inversion of long-term time-lapse electrical resistivity data is challenging. In 2019, the procedure was made more difficult because of the higher reciprocal errors of the replacement instrument, used after May. Difference and background-constrained inversion were tested but both could not reproduce the diurnal dynamics observed in the apparent conductivity data during the entire season and most failed to converge at the end of the growing season. Difference inversion performed well when applied on the data collected before the first nitrogen application but failed to reproduce the variations observed in the apparent values afterwards. Difference inversion is usually effective when the surveys shared a high systematic error and a low random error but
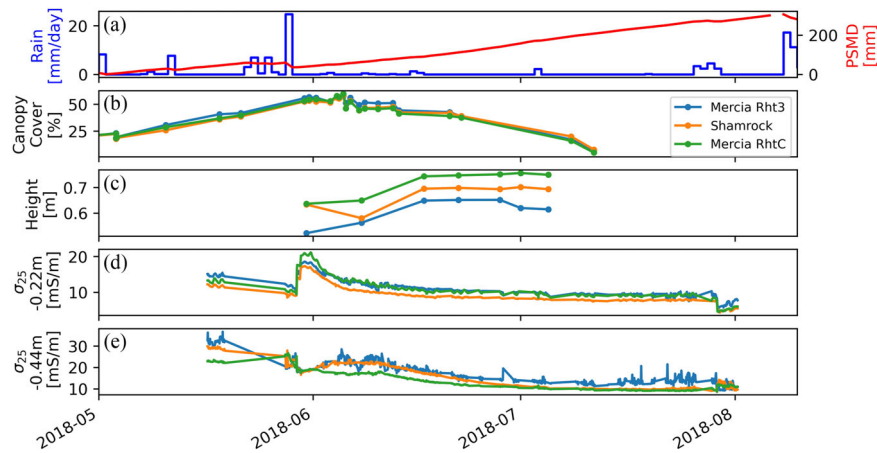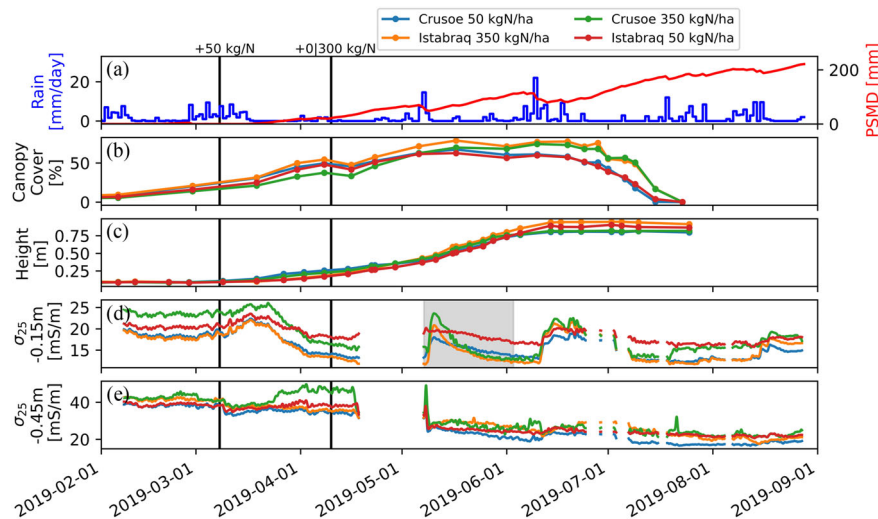
Figure 4 Time course of different variables on the 2018 experiment with three different winter wheat lines (Rht3 Mercia, RhtC Mercia and Shamrock). (a) Daily precipitation and potential soil moisture deficit. (b) Canopy cover development derived from RGB picture. Maximum canopy cover is reached from end of May and senescence start in the beginning of July. Canopy cover does not reach value higher than 80% because of the gaps between the subplots. (c) Increasing height of the crops. (d and e) Inverted temperature corrected electrical conductivity for each variety at 0.22 m and 0.44 m depths, respectively.

that might not be the case in this study. As a simpler approach, each survey was inverted individually with a power-law error model based on the binned reciprocal error of the batch of 24 consecutive surveys. We noticed that the inclusion of an error model greatly helps the inversion to converge and would recommend the addition of reciprocal measurements in automated sequence for this purpose. In applications of difference inversion type schemes, a different type of error model that

reduces systematic errors can be considered (Lesparre *et al.*, 2019).

One important challenge that we met with the inversion of hourly geoelectrical data was to be able to retain the day–night pattern observed in the apparent resistivity measurements following their inversion. In this study, we successfully retrieved this pattern for shallower depths, but we noted that deeper depths do not show similar daily fluctuations (Fig. 5e).

Figure 5 Time course of different variables on the 2019 experiments with two winter wheat varieties (Istabraq and Crusoe) and two different nitrogen treatments (50 and 350 kgN/ha). (a) Daily precipitation and potential soil moisture deficit. (b) Developing canopy cover determined from RGB picture. (c) Increase in crop heights over time. (d and e) Time course of the temperature corrected inverted electrical conductivity under the four crops. Note that a moving average of window 3 has been applied on (d) and (e) to reduce the noise and remove outliers. The shaded area in (d) can be viewed enlarged in Figure 8. The two vertical black lines show when the nitrogen fertilizer was applied (2019-03-08 and 2019-04-10).
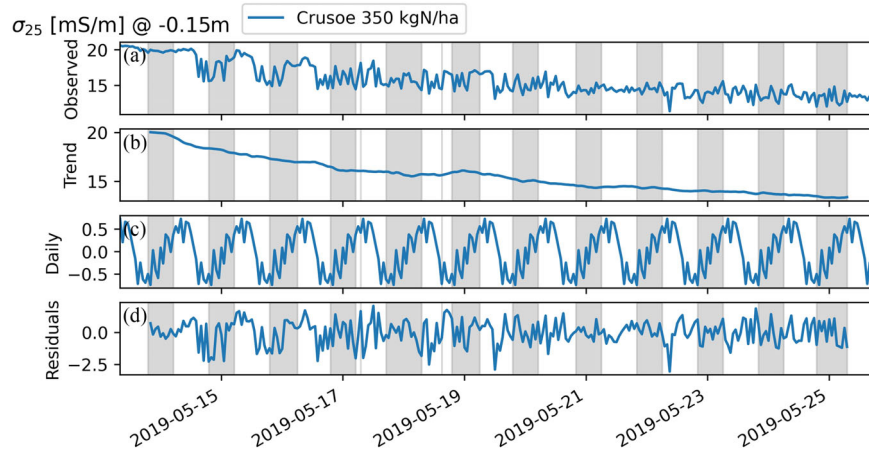
Figure 6 (a) Portion of the temperature corrected inverted conductivity signal at 0.15 m depth after the main rainfall event of mid-May. Shaded areas represent the night. The signal is decomposed in three additive components: the trend (b), the daily component (also called seasonality) (c) and the residuals (d).

Figure 9 compares the evolution of the apparent and inverted values for shallow and deeper depths. Apparent values show a daily pattern for shallow and for deep depths while the daily pattern is only visible in the shallow depth for the inverted values. The current study mainly focuses on shallower depths as they exhibit faster responses to meteorological events but also because most of the root system of winter wheat usually lies above 0.3 m depth (see, for example, Hodgkinson *et al.*, 2017). Without detailed root data for our experiments we have to assume this to be the case here. Additionally, another reason for only observing the daily pattern at shallow depths is the structure of the soil texture. Indeed, the higher clay content of the soil below 0.3 m might have substantially slow down water fluxes and hence attenuated the fluctuations. This is a potential limitation of the current study site and the experiment would benefit from a repeat in a well-drained environment to see if these daily fluctuations can be observed deeper.

Finally, an important factor when measuring hourly electrical conductivity is the effect of soil temperature as shown by the cross-correlation plot of Fig. 2(b). The diurnal pattern of temperature strongly influences electrical conductivity, particularly at shallow depths. Applying the usual temperature correction using the ratio model (equation 1) helps to reduce this effect and decreases the cross-correlation (Fig. 2b).

Coupling with other above-ground variables

In 2018, the different wheat varieties did not show large difference in term of canopy cover which can be attributed to the lack of rain during the canopy expansion phase (Fig. 3b). This might explain why no large difference in the dynamics of the

inverted conductivities were observed between the varieties (Fig. 3d,e). Figure 4(d) shows that the conductivity at −0.22 m under Mercia RhtC decreased slightly faster after a major rainfall event which might be linked to the larger canopy cover of the variety. In other field trials, Hodgkinson *et al.* (2017) observed that the dwarf wheat variety (Mercia Rht3) has a deeper root system but that this does not lead to larger root water uptake. No links could be found between the yield and the dynamics of the electrical conductivity in 2018.

In contrast, large differences in canopy cover were observed in 2019 between the plots. The dynamics of the electrical conductivity is clearly related to the development of the canopy cover when no major rainfall events occur (Fig. 5b,c).

Figure 8 shows that the plots receiving more nitrogen show a larger increase in electrical conductivity during the rainfall event. One explanation could be that part of the nitrogen from the last application was still in the soil in granular form, and not yet in a form available to the crop. With the rainfall, it was dissolved again in the soil solution and caused a surge in the electrical conductivity. We did observe a small peak after the first application of fertilizer (Fig. 5d). Once dissolved, the nitrogen is quickly taken up the roots resulting in a faster decrease of the soil electrical conductivity. Figure 6 This newly absorbed nitrogen can then be allocated to the growth of the crop, leading to an expansion of the canopy cover (Fig. 5d). The decrease in electrical conductivity could also be due the crop water uptake which depends on the canopy cover. However, the rate of uptake of the different crops is likely to be comparable given their similar canopy cover prior to the event. In this study, separating the two effects is difficult without independent measure of the soil moisture.

Figure 7 Evolution of the daily component of the additive model fitted on a several moving windows of a week (seven days) with a two-day offset between consecutive windows. (a) Observed data (here the temperature corrected inverted conductivity at 0.15 m depth) and two windows. The first window of a week is extracted, and the additive decomposition is applied. The cyclic component is displayed in (b). A second window is chosen two days later, and the same process is repeated (c). The shaded area represents night. (d) Evolution of the daily components for each moving window over the whole growing season during night (19–7 h) and day (7–19 h). Moving windows spanning no data intervals have been removed.
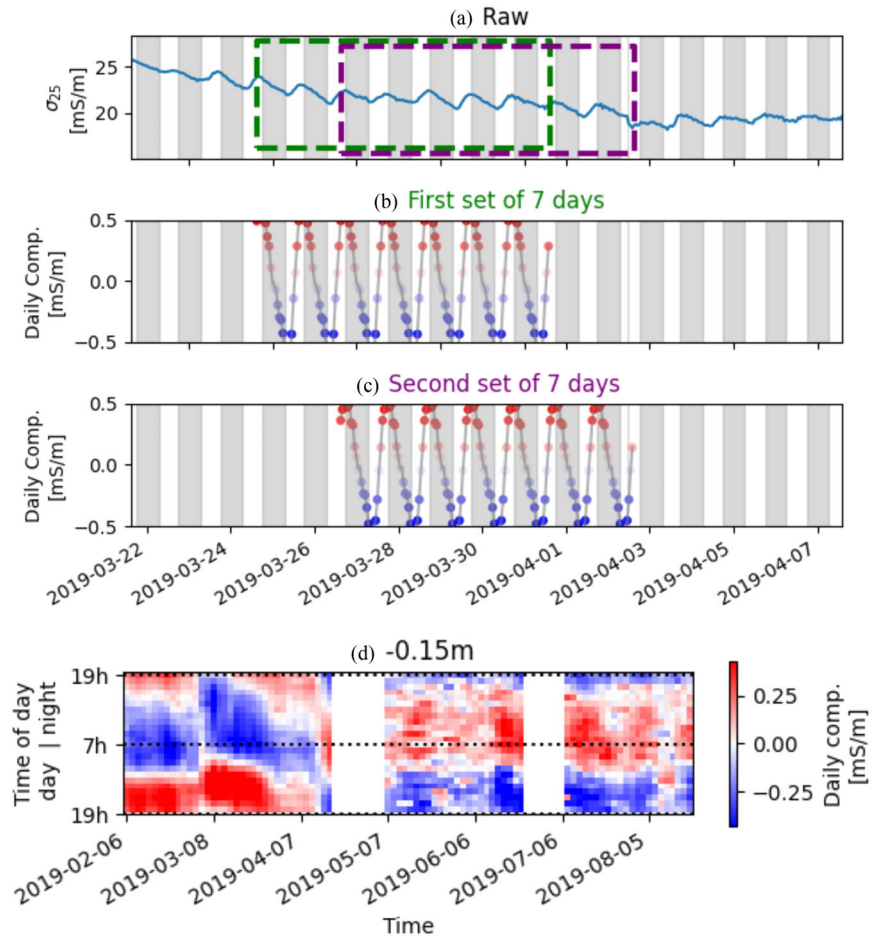

There was no strong correlation between crop height and electrical conductivity. The crop height was more influenced by the variety and less by the nitrogen treatment. In contrast, the yield of the crops which received more nitrogen was much greater compared to those receiving less. However, for a given level of nitrogen (either 50 or 350 kgN/ha), Istabraq shows a slightly higher yield than Cruose. For example, Istabraq 350 kgN/ha has a higher grain yield (13.6 t/ha) than Crusoe 350 kgN/ha (12 t/ha).

Figure 8 Enlargement of the grey shaded area of Figure 5(d) showing the evolution of the inverted conductivity of the four crops under the Scanalyzer in 2019 during and after the major rainfall event at the end of May 2019. Note the faster decrease in electrical conductivity of the crops which received more nitrogen.

Diurnal cycles

As previously stated, no direct measurements of soil moisture content were collected during these two experiments. However, the relationship between the electrical conductivity and the soil moisture content was known for the soil under the Scanalyzer. With it, we can relate the electrical conductivity data from the graphs above to soil moisture content. However, given the suspected contribution of the nitrogen fertilizer
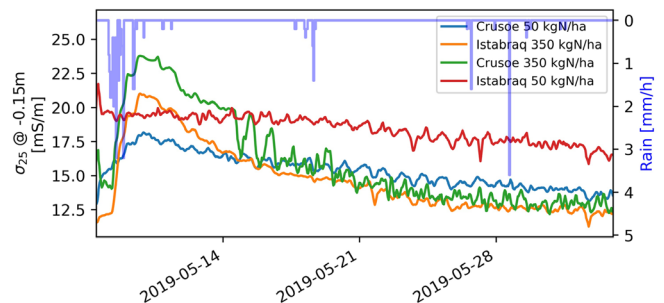
Table 1 Summary of the yield of the different varieties in both years

| Variety Winter Wheat	N Fertilizer	Year	Grain Yield @ 85% (t/ha)	Straw Yield @ 85% (t/ha)	Total Biomass @ 85% (t/ha)
Mercia Rht3	–	2018	2	5.4	7.4
Shamrock	–	2018	5.6	7.9	13.5
Mercia RhtC	–	2018	6.5	8.1	14.6
Crusoe	50 kgN/ha	2019	10	10.7	20.7
Istabraq	50 kgN/ha	2019	10.5	10.1	20.6
Crusoe	350 kgN/ha	2019	12	11.8	23.8
Istabraq	350 kgN/ha	2019	13.6	13.6	27.2

to the electrical conductivity (mainly around large rainfall events), the focus here has been on electrical conductivity variation.

Diurnal patterns are present in the apparent conductivities measured (Fig. 9a,b). Once inverted, and temperature corrected, those diurnal cycles are still visible mainly for shallower depths and attenuated for deeper depths (Fig. 5d,e). In order to see if these patterns are related to crop activity, partitioning of the time series was performed. However, we acknowledge that univocally attributing the changes in electrical conductivity to root water uptake is not possible in this study.

Figure 6(c) shows that the daily component for all the plots tends to decrease during day and increase during night in May. Note that earlier in the season the opposite trend was observed (Fig. 6) when the crop had probably less effect

on the dynamics of the soil moisture. The daily component is arguably noisy, and we explain this partly because of the noise in the original signal (Fig. 6a) but also because this daily component is extracted as the mean of the periodic difference between the raw signal and the trend. One main limitation of the additive decomposition is that the daily component cannot vary in amplitude from one day to another. We hypothesize that this daily component is mainly influenced by the root water uptake of the crop – which follows a diurnal cycle as seen, for instance, in Verhoef *et al.* (2006) or Werban *et al.* (2008). The nightly increase observed from May could be due to soil moisture replenishment or hydraulic lift (Horton and Hart, 1998).

The same decomposition approach was applied on moving windows throughout the whole season (Fig. 7) and revealed a shift from April onward in the daily component of
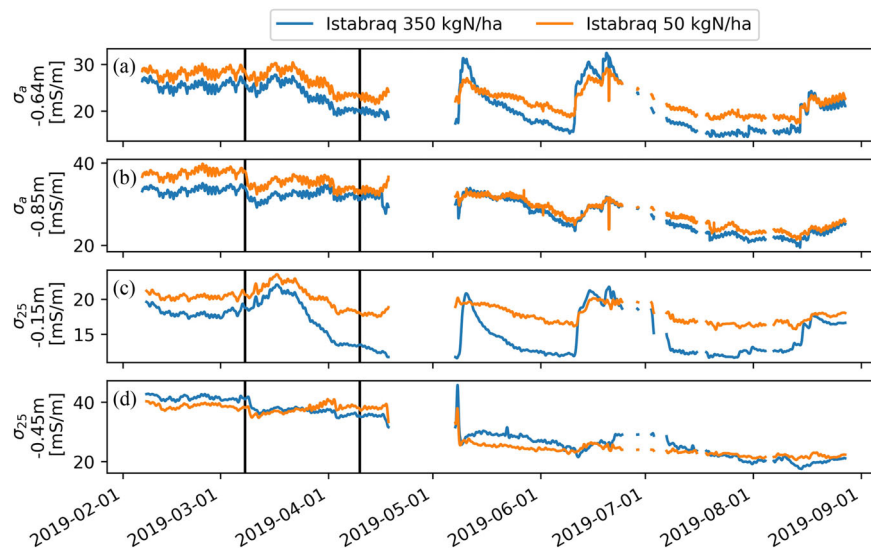
Figure 9 Comparison between two apparent conductivities (a) and (b) and two inverted temperature corrected conductivities (c) and (d) for the two plots of Istabraq in 2019. Both (c) and (d) were smoothed by a moving average (window = 3). Note that the inverted conductivities at deeper depths do not show strong daily fluctuation compared to the apparent resistivity data (compare plot (d) with (b)) but rather an attenuated version of the seasonal dynamics.

the signal. This progressive shift appears at a time when the crops start to grow larger canopy cover and show large decrease in electrical conductivity (Fig. 5d). Note also that the diurnal component of the signal was still strong in February when the crops were small and showed a decreasing electrical conductivity during night time. Such a strong daily component in the signal for earlier dates is unexpected. It could be related to the fact that the temperature correction did not completely remove the cross-correlation between temperature and electrical conductivity (Fig. 2). In this case, there may be a residual effect of the temperature cycle that remains in the series. This effect is overcome later in the season by larger effects of the diurnal soil moisture dynamics.

CONCLUSION

This study shows hourly electrical resistivity monitoring applied to small scale agricultural plots with different wheat varieties and nitrogen treatments. A high cross-correlation with the soil temperature and the hourly electrical conductivity makes it essential for the application of a temperature correction. However, diurnal patterns in the electrical conductivity remains and our analysis suggest that this diurnal pattern is mainly influenced by plant activity particularly when the crops are fully grown. Distinguishing differences between varieties remains challenging, and we did not observe any large differences in electrical conductivity either in 2018 or 2019 experiments. However, the effect of nitrogen uptake could be clearly seen in the dynamics of the electrical conductivity during large rainfall events. We acknowledge the limitation of the approach to monitor a few experimental plots, but we believe that higher time resolution has enabled us to gain deeper insight into soil-plant dynamics than the usual coarser time-lapse monitoring, in particular during large rainfall and subsequent drying events but also at the daily scale. Specifically, the ERT monitoring system provided non-invasive depth-specific information that can be related to some above-ground measurements. As such, it offers a unique perspective into the soil-water-plant interactions which is essential for breeding more resilient varieties.

DATA AVAILABILITY STATEMENT

The data that support the findings of this study are available from the corresponding author upon reasonable request.

ORCID

Guillaume Blanchy
https://orcid.org/0000-0001-6341-5826
Nicolas Virlet https://orcid.org/0000-0001-6030-4282
Pouria Sadeghi-Tehran
https://orcid.org/0000-0003-0352-227X
Christopher W. Watts
https://orcid.org/0000-0002-7223-1444
Malcolm J. Hawkesford
https://orcid.org/0000-0001-8759-3969
William R. Whalley
https://orcid.org/0000-0003-0755-2943
Andrew Binley https://orcid.org/0000-0002-0938-9070

REFERENCES

Araus, J.L. and Cairns, J.E. (2014) Field high-throughput phenotyping: the new crop breeding frontier. *Trends in Plant Science*, 19(1), 52–61.

Atkinson, J.A., Pound, M.P., Bennett, M.J. and Wells, D.M. (2019) Uncovering the hidden half of plants using new advances in root phenotyping. *Current Opinion in Biotechnology*, 55, 1–8.

Binley, A. (2015) 11.08 - tools and techniques: electrical methods. In: Schubert, G. (Ed.) *Treatise on Geophysics*, 2nd edition. Oxford: Elsevier, pp. 233–259.

Binley, A., Hubbard, S.S., Huisman, J.A., Revil, A., Robinson, D.A., Singha, K. and Slater, L.D. (2015) The emergence of hydrogeophysics for improved understanding of subsurface processes over multiple scales: the emergence of hydrogeophysics. *Water Resources Research*, 51(6), 3837–3866.

Blanchy, G., Saneiyan, S., Boyd, J., McLachlan, P. and Binley, A. (2020) ResIPy, an intuitive open source software for complex geoelectrical inversion/modeling. *Computers & Geosciences*, 137, 104423.

Cassiani, G., Boaga, J., Vanella, D., Perri, M.T. and Consoli, S. (2015) Monitoring and modelling of soil–plant interactions: the joint use of ERT, sap flow and eddy covariance data to characterize the

volume of an orange tree root zone. *Hydrology and Earth System Sciences*, 19(5), 2213–2225.

Consoli, S., Stagno, F., Vanella, D., Boaga, J., Cassiani, G. and Roccuzzo, G. (2017) Partial root-zone drying irrigation in orange orchards: effects on water use and crop production characteristics. *European Journal of Agronomy*, 82, 190–202.

Corwin, D.L. and Lesch, S.M. (2005) Characterizing soil spatial variability with apparent soil electrical conductivity. *Computers and Electronics in Agriculture*, 46(1–3), 103–133.

Coussement, T., Maloteau, S., Pardon, P., Artru, S., Ridley, S., Javaux, M. and Garré, S. (2018) A tree-bordered field as a surrogate for agroforestry in temperate regions: where does the water go? *Agricultural Water Management*, 210, 198–207.

Furbank, R.T. and Tester, M. (2011) Phenomics – technologies to relieve the phenotyping bottleneck. *Trends in Plant Science*, 16(12), 635–644.

Hayashi, M. (2004) Temperature-electrical conductivity relation of water for environmental monitoring and geophysical data inversion. *Environmental Monitoring and Assessment*, 96(1–3), 119–128.

Hayley, K., Bentley, L.R., Gharibi, M. and Nightingale, M. (2007) Low temperature dependence of electrical resistivity: implications for near surface geophysical monitoring. *Geophysical Research Letters*, 34(18). https://doi.org/10.1029/2007GL031124.

Hodgkinson, L., Dodd, I.C., Binley, A., Ashton, R.W., White, R.P., Watts, C.W. and Whalley, W.R. (2017) Root growth in field-grown winter wheat: some effects of soil conditions, season and genotype. *European Journal of Agronomy*, 91, 74–83.

Horton, J.L. and Hart, S.C. (1998) Hydraulic lift: a potentially important ecosystem process. *Trends in Ecology & Evolution*, 13(6), 232–235.

Jayawickreme, D.H., Dam, R.L.V and Hyndman, D.W. (2008) Subsurface imaging of vegetation, climate, and root-zone moisture interactions. *Geophysical Research Letters*, 35(18). https://doi.org/10.1029/2008GL034690.

LaBrecque, D.J. and Yang, X. (2001) Difference inversion of ERT Data: a fast inversion method for 3-D in situ monitoring. *Journal of Environmental & Engineering Geophysics*, 6(2), 83–89.

Lesparre, N., Robert, T., Nguyen, F., Boyle, A. and Hermans, T. (2019) 4D electrical resistivity tomography (ERT) for aquifer thermal energy storage monitoring. *Geothermics*, 77, 368–382.

Ma, R., McBratney, A., Whelan, B., Minasny, B. and Short, M. (2011) Comparing temperature correction models for soil electrical conductivity measurement. *Precision Agriculture*, 12(1), 55–66.

Mares, R., Barnard, H.R., Mao, D., Revil, A. and Singha, K. (2016) Examining diel patterns of soil and xylem moisture using electrical resistivity imaging. *Journal of Hydrology*, 536, 327–338.

Michot, D., Benderitter, Y., Dorigny, A., Nicoullaud, B., King, D. and Tabbagh, A. (2003) Spatial and temporal monitoring of soil water content with an irrigated corn crop cover using surface electrical resistivity tomography: soil water study using electrical resistivity. *Water Resources Research*, 39(5). https://doi.org/10.1029/2002WR001581.

Prasanna, B.M., Araus, J.L., Crossa, J., Cairns, J.E., Palacios, N., Das, B. and Magorokosho, C. (2013) High-throughput and precision phenotyping for cereal breeding programs. In: Gupta, P. K. and Varshney, R. K. (Eds.) *Cereal Genomics II*. Dordrecht: Springer, pp. 341–374.

Rücker, C. and Günther, T. (2011) The simulation of finite ERT electrodes using the complete electrode model. *Geophysics*, 76(4), F227–F238.

Sadeghi-Tehran, P., Virlet, N., Sabermanesh, K. and Hawkesford, M.J. (2017) Multi-feature machine learning model for automatic segmentation of green fractional vegetation cover for high-throughput field phenotyping. *Plant Methods*, 13(1), 103.

Seabold, S. and Perktold, J. (2010) Statsmodels: econometric and statistical modeling with Python. 92 *Proceedings of the 9th Python in Science Conference (SCIPY 2010)*.

Senapati, N. and Semenov, M.A. (2020) Large genetic yield potential and genetic yield gap estimated for wheat in Europe. *Global Food Security*, 24, 100340.

Sheets, K.R. and Hendrickx, J.M.H. (1995) Noninvasive soil water content measurement using electromagnetic induction. *Water Resources Research*, 31(10), 2401–2409.

Srayeddin, I. and Doussan, C. (2009) Estimation of the spatial variability of root water uptake of maize and sorghum at the field scale by electrical resistivity tomography. *Plant and Soil*, 319(1–2), 185–207.

Vanella, D., Cassiani, G., Busato, L., Boaga, J., Barbagallo, S., Binley, A. and Consoli, A. (2018) Use of small scale electrical resistivity tomography to identify soil-root interactions during deficit irrigation. *Journal of Hydrology*, 556, 310–324.

Verhoef, A., Fernández-Gálvez, J., Diaz-Espejo, A., Main, B.E. and El-Bishti, M. (2006) The diurnal course of soil moisture as measured by various dielectric sensors: effects of soil temperature and the implications for evaporation estimates. *Journal of Hydrology*, 321(1), 147–162.

Virlet, N., Sabermanesh, K., Sadeghi-Tehran, P. and Hawkesford, M.J. (2017) Field scanalyzer: an automated robotic field phenotyping platform for detailed crop monitoring. *Functional Plant Biology*, 44(1), 143.

Werban, U., al Hagrey, S.A. and Rabbel, W. (2008) Monitoring of root-zone water content in the laboratory by 2D geoelectrical tomography. *Journal of Plant Nutrition and Soil Science*, 171(6), 927–935.

Whalley, W.R., Binley, A., Watts, C.W., Shanahan, P., Dodd, I.C., Ober, E.S., Ashton, R.W., Webster, C.P., White, R.P. and Hawkesford, M.J. (2017) Methods to estimate changes in soil water for phenotyping root activity in the field. *Plant and Soil*, 415(1–2), 407–422.